Relaxations of the surface photovoltage effect on the atomically controlled semiconductor surfaces studied by time-resolved photoemission spectroscopy

M. Ogawa,[1] S. Yamamoto,[1] K. Fujikawa,[1] R. Hobara,[1] R. Yukawa,[1] Sh. Yamamoto,[1] S. Kitagawa,[2] D. Pierucci,[3] M. G. Silly,[3] C.-H. Lin,[4] R.-Y. Liu,[4] H. Daimon,[2] F. Sirotti,[3] S.-J. Tang,[4] and I. Matsuda[1,*]

[1]*Institute for Solid State Physics, The University of Tokyo, 5-1-5 Kashiwanoha, Kashiwa, Chiba 277-8581, Japan*
[2]*Nara Institute of Science and Technology (NAIST), Ikoma, Nara 630-0192, Japan*
[3]*TEMPO Beamline, Synchrotron Soleil, L'Orme des Merisiers Saint-Aubin Boîte Postale 48 91192 Gif-sur-Yvette Cedex, France*
[4]*Department of Physics and Astronomy, National Tsing Hua University, Hsinchu 30013, Taiwan*

We have systematically investigated relaxation of the surface photovoltage effect on the atomically controlled In/Si(111) surfaces with distinctive surface states and different amounts of the surface band bending. The temporal variations were traced in *real time* by time-resolved photoemission spectroscopy using soft x-ray synchrotron radiation. The relaxation is found to be temporally limited by two steps of the carrier transfer from the bulk to the surface: the tunneling process at a delay time $\leqslant 100$ ns and the thermionic process on the following time scale ($\geqslant 100$ ns). Crossover of the two mechanisms can be understood by breakdown of the quantum tunneling regime by the increase in width of the space-charge layer during the relaxation.

I. INTRODUCTION

Research in photoscience, especially photovoltaics and photocatalysis, has become important in dealing with global energy issues. The photovoltage effect is the basic process in photovoltaics and photocatalysis, and has drawn considerable interest in both fundamental and applied physics.[1,2] In the surface photovoltage (SPV) effect,[3] an electron-hole pair created by photoexcitation is split and the two types of carriers are spatially separated, as schematically shown in Fig. 1(a),1(b). The electron-hole separation is induced by their opposite drift forces near the surface, creating a voltage difference between the surface and bulk. On the other hand, the SPV effect is relaxed by electron-hole recombination at the surface after diffusion of one of the carriers from the bulk. It has been argued that the carrier transport proceeds by thermodynamically transferring over the surface potential barrier or by quantum-mechanically tunneling through it [Figs. 1(c) and 1(d)].[4–6]

Carrier dynamics during generation and relaxation of the SPV effect have been empirically probed by various time-resolved measurement methods, such as photoluminescence, reflection, and photoelectron spectroscopies.[7–11] Photoemission measurements have an advantage in being able to trace electronic states (valence bands or molecular orbitals) and chemical shifts (core-level states) directly[12,13] in *real time*. Recently, there have been several time-resolved photoemission experiments[6,14–20] on the SPV effect on semiconductor surfaces. These studies have revealed the important role of a surface in relaxation of the SPV effect. Surfaces have been known to change their electronic properties significantly even with submonolayer adsorption of foreign atoms.[21–24] Thus, it is inferred that relaxation of the SPV effect is significantly sensitive to surface characteristics that can be regulated by surface treatments.

In the present research, we performed time-resolved photoemission spectroscopy (TRPES) of the In/Si(111) surface system to trace relaxation of the surface photovoltage effect. The carrier dynamics is investigated on the eight surfaces, as listed in Table I, with varying indium coverage, long-range order, electronic structure, atomic structure, and surface potential (amount of band bending). The time evolution depends on the surfaces and the relaxation essentially proceeds in two steps: a fast process at the initial stage and the following slow process. The former and latter can be described in terms of the tunneling and the thermionic relaxation schemes, respectively [Figs. 1(c) and 1(d)]. The transition between the two mechanisms was found at a certain amount of the surface potential, which likely corresponds to the critical width for the tunneling transport. The crossover can be understood by breakdown of the quantum tunneling regime by the increase in width of the space-charge layer (SCL) during the relaxation.

II. EXPERIMENT

The photoemission experiment was performed at room temperature at beamline BL07LSU at the synchrotron radiation (SR) facility SPring-8 and at the TEMPO beamline at SOLEIL.[25–28] The time-resolved data were obtained using the pump (laser) and probe (SR) method. The laser and SR pulse durations were about 35 fs and 50 ps, respectively. The pumping laser was set to provide a photon energy ($h\nu$) of $h\nu = 1.51$ eV with a repetition rate of 1 kHz. Time evolution of the nonequilibrium carrier relaxation was traced by measuring Si $2p$ core-level spectra, taken at $h\nu \sim 252$ eV, at various delay times after the laser irradiation to induce the SPV effect.

A clean Si(111) 7×7 surface was prepared on a heavily doped n-type ($\rho = 0.02$ Ω cm) Si(111) wafer by a cycle of *in situ* resistive heating treatments. Indium deposition was performed with a Knudsen-cell-type evaporator. Ordered surface phases of In/Si(111) were prepared[32–38] by In deposition at room temperature (RT), followed by annealing at 673 and 773 K. The $\sqrt{3} \times \sqrt{3}$, $\sqrt{31} \times \sqrt{31}$, and 4×1 phases were formed with In coverages of 1/3, 1/2, and 1 ML, respectively (1 ML $= 7.8 \times 10^{14}$ atoms/cm^2). The quality of the surfaces was ascertained by sharp patterns of low-energy electron diffraction (LEED). For comparison, surfaces prepared by In deposition at RT were also examined. Figure 2 shows the In
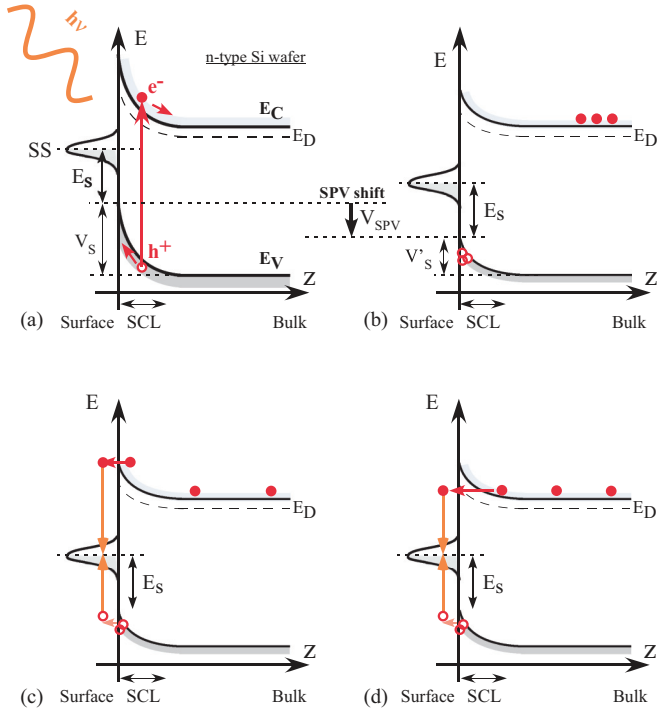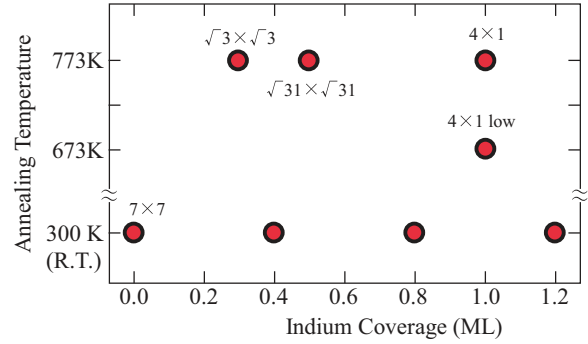
FIG. 2. (Color online) Summary of the eight sample surfaces prepared with different In coverages and annealing temperatures. The surfaces with long-range orders are labeled with the names of the phases. The Si(111)4 × 1-In surfaces, prepared by room-temperature deposition and postannealing at 673 and 773 K are labeled "4 × 1 low" and 4 × 1, respectively.

FIG. 1. (Color online) (a), (b) Evolution of the SPV effect and the following relaxation through the (c) thermionic and (d) tunneling processes. E_C and E_V are the energies of conduction and valence band edges, respectively, while E_D is the energy position of the donor level. The energy level E_S of a surface state (SS), is referred from E_V at a surface. The surface potential (V_S) is equivalent to the amount of band bending and the energy shift after SPV is indicated with V_{SPV}. The region of a space-charge layer (SCL) is indicated with an arrow.

coverage versus annealing temperature for the formation of eight surface samples investigated in the present research.

III. RESULTS AND DISCUSSION

A. Physical properties of the In/Si(111) surfaces

Crystal surfaces are known to form many long-range ordered phases, so-called surface superstructures, through different combinations of substrates, adsorbates, temperatures, and preparation procedures.[21,22] There are various In/Si(111) phases at RT that show distinctive atomic and electronic

structures.[32–38] A pristine surface before In deposition is the metallic Si(111)7 × 7 surface that has the atomic arrangement of a dimer-adatom-stacking fault model.[38,39] For an In coverage of 1/3 ML, the $\sqrt{3} \times \sqrt{3}$-In surface phase is formed by heat treatment (Fig. 2) and the surface is known to be semiconducting.[38] At 1/2 ML, the $\sqrt{31} \times \sqrt{31}$ phase can be observed after annealing above 673 K. Surface structures of $\sqrt{3} \times \sqrt{3}$ and $\sqrt{31} \times \sqrt{31}$ phases have been reported elsewhere.[35,38] The 4 × 1-In phase completely covers the Si(111) surface at the In coverage of 1 ML. The Si(111)4 × 1-In surface is composed of an array of In chains and has quasi-one-dimensional metallic bands, indicating that the surface is one-dimensional (1D) metallic.[36,37] Thus, with the difference in In coverage on the Si(111) surface, one can prepare long-range ordered surfaces with distinctive surface atomic structures and electronic states (Table I).

Variations in the surface electronic structures or the surface density of states change the amount of bulk band bending near the surface, V_S, through the charge neutrality condition.[22–24] Figure 3 compares the binding energies of the Si $2p$ core level among various In/Si(111) surfaces. It has been known that the relative energy position of the core level matches those of bulk valence and conduction band edges.[6,14–20] In Fig. 3, the position of the Si $2p_{3/2}$ peak of 7 × 7 is marked as the dashed line and taken as the reference of the relative binding energy on

TABLE I. Parameters of sample surfaces used in the present research. 1 ML (monolayer) corresponds to the Si(111) surface atomic density, 7.8×10^{14} atoms/cm². The E_S value of the 7 × 7 phase was taken from the references (Refs. 29–31).

| Surface	Coverage (ML)	Surface order	Electronic structure	E_S (eV)	V_S (eV)	$E_S - E_i$ (eV)	SCL
7 × 7	0.0	Ordered	2D metal	0.63 (Ref.)	0.37	0.085	Depletion
$\sqrt{31} \times \sqrt{31}$	0.5	Ordered		0.60	0.40	0.051	Depletion
$\sqrt{3} \times \sqrt{3}$	0.3	Ordered	Semiconductor	0.55	0.45	0.009	Depletion
RT deposited	0.4	Disordered		0.49	0.51	−0.052	Inversion
RT deposited	0.8	Disordered		0.42	0.58	−0.13	Inversion
RT deposited	1.2	Disordered		0.44	0.56	−0.105	Inversion
4 × 1 low	1.0	Ordered	1D metal	0.36	0.64	−0.185	Inversion
4 × 1	1.0	Ordered	1D metal	0.32	0.68	−0.225	Inversion
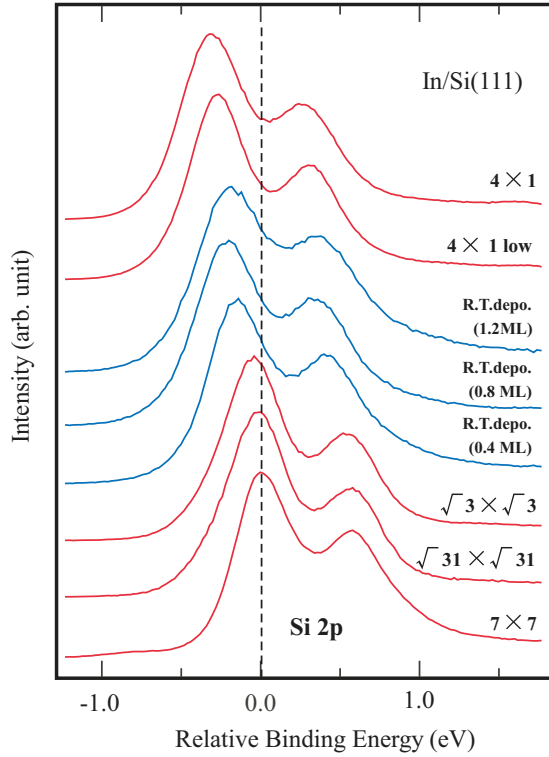
FIG. 3. (Color online) Si $2p$ core-level spectra of various In/Si(111) surfaces, as listed in Table I, taken at a photon energy of 252 eV. Each spectrum is labeled with the corresponding sample surface. The dashed black line marks the peak position of the Si(111)7×7 surface.

the horizontal axis. The binding energies corresponding to the In-covered surfaces are lower than those of the Si(111)7×7 surface.

The surface Fermi level from the valence band edge of the Si(111)7×7 surface is reported to be $E_F - E_V = E_s = 0.63$ eV.[29–31] Taking this value as the reference, one can determine the surface Fermi level of the individual surface shown in Fig. 3. Table I gives the surface Fermi level E_S, amount of band bending V_S, and $E_S - E_i$ for the In/Si surfaces, where E_i is intrinsic energy. For example, V_S changes by ~ 300 meV in the transition from the clean 7×7 phase to the 4×1-In phase. SCL classification is also shown in Table I. According to the definition,[22] the 7×7, $\sqrt{31} \times \sqrt{31}$, and $\sqrt{3} \times \sqrt{3}$ surfaces are of the depletion type, while the rest of the surfaces are of the inversion type.

B. SPV effect

Moving on to the photoemission spectra taken after the photoexcitation, Fig. 4 plots the energy variation in the Si $2p$ core-level spectra obtained with various power densities of the pumping laser at a delay time of 1 ns. The energy shift initially increases logarithmically with the power density but deviates above ~ 10 μJ/cm^2/pulse. Above ~ 100 μJ/cm^2/pulse, the power dependence saturates. The dependence of the surface photovoltage on laser power density is similar to those reported for other semiconductor surfaces.[6,14,19]
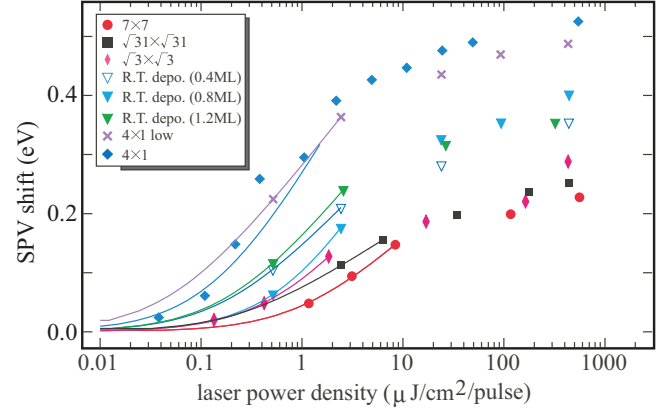

FIG. 4. (Color online) SPV shift for each surface phase and fitting with Eq. (1). The difference in the amount of shift comes from the difference in surface charge in the stationary state, i.e., the band bending in the initial state.

In general, the SPV effect increases with more photoexcited electrons and holes. Thus, the SPV shift becomes large with an irradiating photon flux. The power dependence of the energy shift due to light illumination (V_{SPV}) can be written as[6]

$$V_{SPV} = \eta kT \ln(1 + \gamma I), \tag{1}$$

where I is the laser power, γ is the proportional factor, and η is the ideality factor.[4] Below $I \sim 10$ μJ/cm^2/pulse, the data can be fitted well with Eq. (1), indicating the typical SPV regime in the region. Values of η are in the range 3.5 ± 1.5, while the range of γ is 10 ± 10. The fitting results show that the two parameters tend to take larger values for greater band bending (V_S). Above $I \sim 100$ μJ/cm^2/pulse, the SPV shift shows the saturating behavior and, thus, the simple SPV theory is no longer valid. We note that the peak positions of the Si $2p_{3/2}$ core level for all the surfaces saturate at the same energy when they are plotted in binding energy. This indicates a non-surface-specific property and the phenomenon likely corresponds to the flat band condition for the bulk band. In the following, we used TRPES to trace temporal variations after the SPV effect on the In/Si(111) surfaces, pumped optically with a power density below $I \sim 10$ μJ/cm^2/pulse.

C. Relaxation of the SPV effect

As an example, Fig. 5 displays a series of TRPES spectra of the Si $2p_{3/2}$ level at various delay times for the Si(111)$\sqrt{3} \times \sqrt{3}$-In surface. Figure 6 shows plots of the energy shift of the Si $2p_{3/2}$ level at various delay times for surfaces of (a) Si(111)$\sqrt{3} \times \sqrt{3}$-In and (b) Si(111)4×1-In. The energy shift was measured relative to the energy position before the pumping. While the relaxation completes by 1000 ns on Si(111)$\sqrt{3} \times \sqrt{3}$-In, it continues over 7000 ns on Si(111)4×1-In. The binding energy of the core level moves toward the original position in two steps: a fast process at a delay time $\leqslant 100$ ns and slow process at $\geqslant 100$ ns.

In analyzing relaxations, an experimentalist typically uses an exponential function and obtains the relaxation time τ from

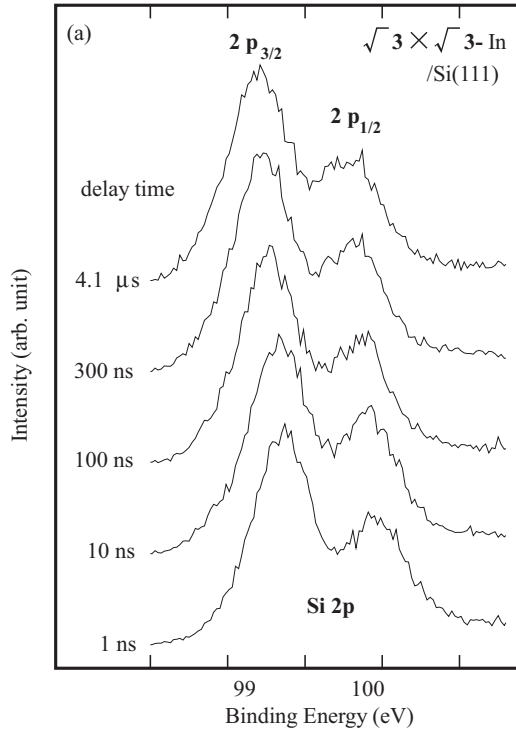FIG. 5. Evolution in TRPES spectra of Si(111)$\sqrt{3} \times \sqrt{3}$ In taken at various delay times after the SPV effect, induced with a laser power density of 3.1 μJ/cm^2/pulse.

the gradient of the data points plotted in logarithmic scale:

$$f(t) = A \exp\left(-\frac{t}{\tau}\right), \quad (2)$$

where $f(t)$ represents a physical quantity which has exponential time dependence and A is a prefactor constant. Figure 7 shows the logarithmic plots of the data for the (a) Si(111)$\sqrt{3} \times \sqrt{3}$-In and (b) Si(111)4 $\times$ 1-In surfaces, shown
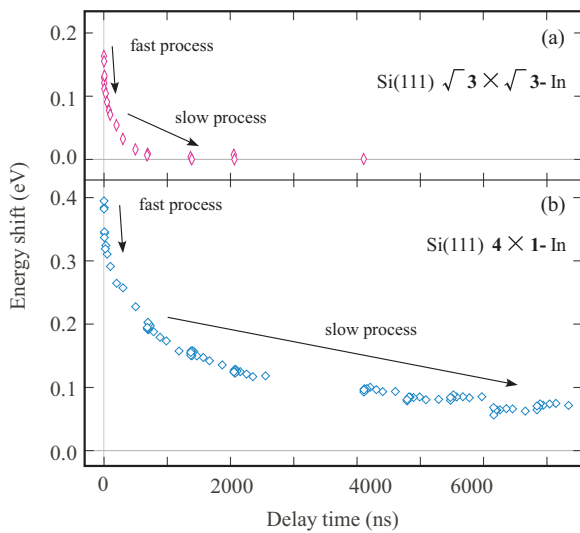

FIG. 6. (Color online) Energy shift of peak position of Si 2 $p_{3/2}$ with delay time on (a) Si(111)$\sqrt{3} \times \sqrt{3}$ In and (b) Si(111)4 $\times$ 1 In. The vertical axis represents relative binding energy with respect to the Si 2$p_{3/2}$ peak position before the photoexcitation.
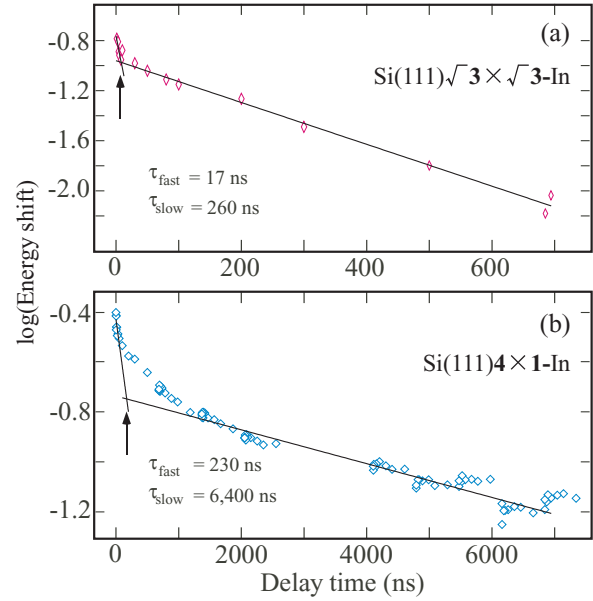

FIG. 7. (Color online) Logarithmic energy shift for the peak position of Si 2 $p_{3/2}$ with delay time on (a) Si(111)$\sqrt{3} \times \sqrt{3}$ In and (b) Si(111)4 $\times$ 1 In. The linear curve fits are made for the fast and slow processes. The time constants are given in the figure. In each figure, crossing points of the two extrapolated lines are indicated by an arrow.

in Fig. 6. Data points in the time regions of the fast and slow processes, described in Fig. 6, can individually be curve fitted by lines and their relaxation times are obtained. The crossover of the two processes may be characterized by the crossing point of the extrapolated lines, which is indicated by an arrow in Fig. 7.

While the exponential analysis is concise to obtain the phenomenological overall picture of the relaxation, it is often insufficient to understand details of the relaxation mechanism. As mentioned in Fig. 1, relaxation of the SPV effect has been theoretically understood as caused by surface recombination of carriers (electrons and holes) that are transferred from the bulk to the surface through or over the surface potential barrier.[4–6] The former is the tunneling transport model.[4,5,40–44] When free carriers in the bulk tunnel through the surface potential barrier to a state at the surface, followed by the surface recombination, the decay (recombination) rate is governed by overlaps of their wave functions. The carrier kinetic equation is

$$\frac{dN(z,t)}{dt} = -\frac{N(z,t)}{\tau_{\text{tunnel}}} \exp\left(-\frac{2z}{a_e}\right), \quad (3)$$

where z is the tunneling distance and the τ_{tunnel} is the time constant. a_e is the Bohr-type radius of the electronic state at the surface that captures electrons from the bulk. Then, the time dependence of the energy shift, $V_{\text{tunnel}}(t)$, is expressed as (see the Appendix)

$$V_{\text{tunnel}}(t) = \frac{e^2}{2\epsilon\epsilon_0} n d^2 \left[\left(1 - \frac{a_e}{2d}\right)^2 \ln^2\left(1 + \frac{t}{\tau_{\text{tunnel}}}\right)\right], \quad (4)$$

where ϵ_0 and ϵ are the dielectric permittivity for vacuum and relative permittivity, d is the mean width of a space-charge layer, and e is the elementary charge.
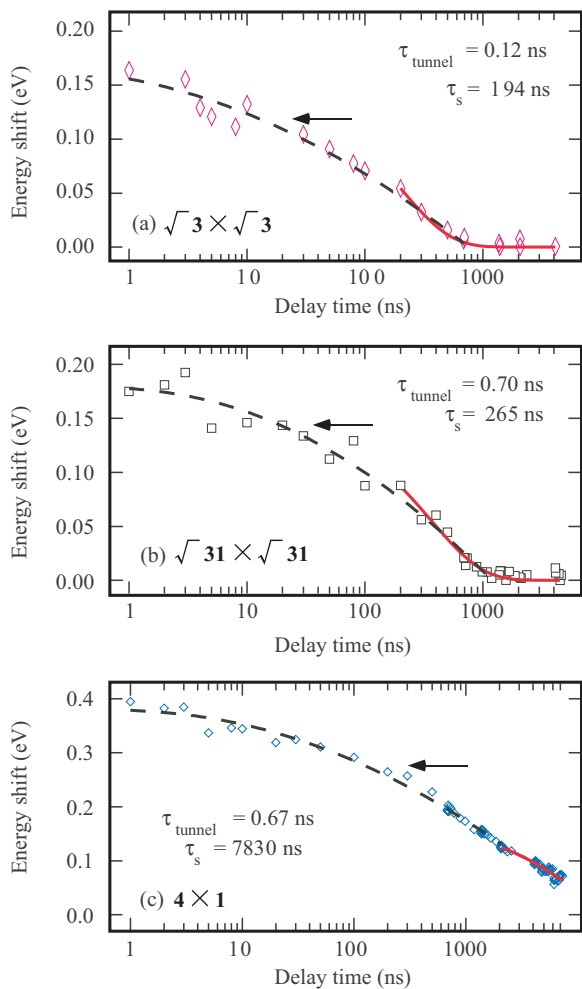
FIG. 8. (Color online) Measured relaxation process of (a) $\sqrt{3} \times \sqrt{3}$, (b) $\sqrt{31} \times \sqrt{31}$, and (c) 4 × 1. All the data were taken with a laser power of 3.1 μJ/cm^2/pulse. The (red) solid and (black) broken lines are the curve fits for thermionic emission [Eq. (5)] and tunneling [Eq. (4)], respectively. The time constants of the thermal diffusion and tunneling diffusion models for the surfaces are given in the figure. In each figure, crossing points of the two extrapolated lines are indicated by an arrow.

On the other hand, the latter model corresponds to thermionic emission:[4–6,43]

$$V_{\text{thermal}}(t) = \eta kT \ln\left[1 - \left(1 - e^{V_{SPV}(0)/\eta kT}\right) e^{-t/\tau_s}\right], \quad (5)$$

where k is the Boltzmann constant, T is absolute temperature, and $V_{SPV}(0)$ is the initial surface photovoltage. Again η is the ideality factor,[4,6] and τ_s corresponds to the (dark) carrier lifetime before the laser irradiation.[6,43]

Figures 8 and 9 show examples of the measured decays of the SPV shift versus the delay time on a logarithmic scale for each surface phase. While the 0.8 ML-RT-deposited and the 4 × 1 surfaces do not complete the relaxation within the measured range, the rest of the surfaces complete it. The (red) solid and (black) broken lines are the curve fits of thermionic emission [Eq. (5)] and tunneling [Eq. (4)], respectively. The time constants τ_{tunnel} and τ_s of the In/Si(111) surfaces are individually given in Figs. 8 and 9. From the curve fit, η was about 2, which is similar to those reported previously.[6,45] For
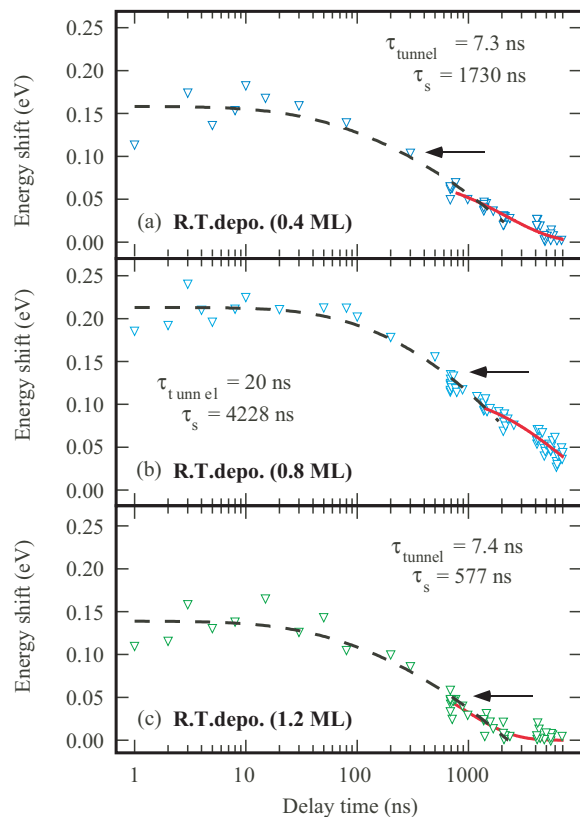

FIG. 9. (Color online) Measured relaxation process of (a) 0.4, (b) 0.8, and (c) 1.2 ML deposition surfaces. The excitation laser power is 3.1 μJ/cm^2/pulse for the 0.8 ML deposition surface, and 0.52 μJ/cm^2/pulse for the 0.4 and 1.2 ML deposition surfaces. The (red) solid and (black) broken lines are the curve fits of thermionic emission [Eq. (5)] and tunneling [Eq. (4)], respectively. The time constants of the thermal diffusion and tunneling diffusion models for the surfaces are given in the figure. In each figure, crossing points of the two extrapolated lines are indicated by an arrow.

all three figures we found that the data could not be fitted with only one of the functions, but were well fitted with their combination: $V_{\text{tunnel}}(t)$ for the shorter delay time and $V_{\text{thermal}}(t)$ for the longer delay time. This behavior indicates that the carriers take either the thermal or tunneling channel to transfer to the surface.

Figure 8 presents the time dependence of the energy shift for the (a) $\sqrt{3} \times \sqrt{3}$-In, (b) $\sqrt{31} \times \sqrt{31}$-In, and (c) 4 × 1-In surface phases. The behaviors of the Si(111)$\sqrt{3} \times \sqrt{3}$-In and the $\sqrt{31} \times \sqrt{31}$-In surfaces are similar to one another, and the time constants are in the subnanosecond range for τ_{tunnel} and several 100 ns for τ_s. We note that the latter is a much longer time scale than the former, which in the relaxation model, is imposed by an exponential factor of the spatial overlap of the wave functions as described in Eq. (3).[43] During the decay of the SPV shift of the 4 × 1-In phase in Fig. 8(c), τ_{tunnel} is 0.67 ns and τ_s is 7830 ns. As shown in Fig. 9, τ_{tunnel} and τ_s are as long as 10 and 1000 ns (1 μs), respectively, on the (a) 0.4, (b) 0.8, and (c) 1.2 ML RT-deposited In/Si surfaces.

At first, the slow decay process, which was well described by time-dependent curves of the thermionic process, is discussed. Figures 10(a) and 10(c) compare the experimental
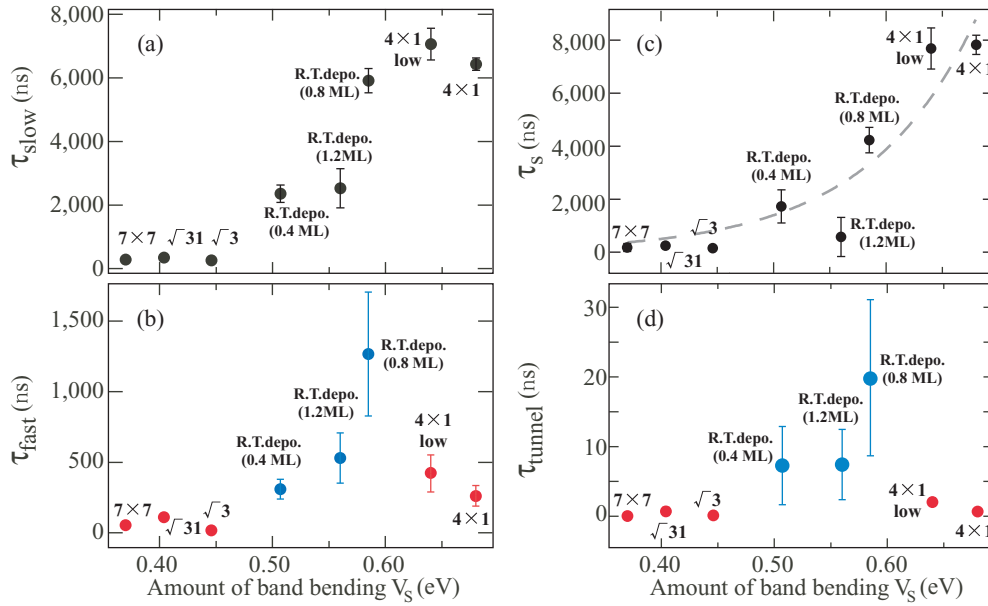
FIG. 10. (Color online) V_S dependence of the time constants of (a) τ_{slow}, (b) τ_{fast}, (c) τ_s, and (d) τ_{tunnel} plotted against V_S. The data points of τ_s are well fitted with an exponential function (broken line). The sample surfaces are labeled.

time constants τ_{slow} and τ_s among the various In/Si(111) surfaces at the corresponding amounts of band bending, V_S. It is obvious that two kinds of the carrier lifetime show the same dependence, becoming long when V_S or the surface potential is large. This can be confirmed by the well-fitting experimental data in Figs. 8 and 9 and it is consistent with the concept of the thermionic process, Fig. 1(c): When the potential barrier is higher, it takes a thermodynamically longer time to transfer over it. This consistency confirms again that the thermionic emission is the slow process, and agrees with previous work.[6] It is of note that τ_s increases exponentially with V_S, as found in Fig. 10(c).

Moving on to the fast decay process, the fast decay time and the time constant of the tunneling model are plotted against V_S in Figs. 10(b) and 10(d), respectively. Two time constants obtained separately, τ_{fast} and τ_{tunnel}, show very similar dependence on V_s. The time constant τ_{tunnel} shows a different dependence from that of τ_s in Fig. 10(c). While the τ_{tunnel} values of the ordered surfaces range from subnanoseconds to nanoseconds, those of the RT-deposited surfaces are as long as 10 ns. It is likely that the disordered surfaces have longer time constants, τ_{tunnel}'s, than those of the ordered surfaces. We note that the 4×1-In phase prepared at 773 K has a better surface order than that prepared at 673 K, as judged from the LEED pattern. Figure 10 shows a longer τ_{tunnel} for "4×1 low" than for 4×1, supporting the relation between the surface disorder and the long τ_{tunnel}. The fitted parameters d, a_e, and n in Eq. (4), for all the surfaces are 10–20 nm, ~ 5 nm, and 10^{11} cm^{-3}, respectively. The SCL width matches those (10–20 nm) calculated from V_S for the present heavily doped n-type Si wafer.

As shown above, the observed relaxation of the surface photovoltage effect was accompanied with the fast and slow processes that can be assigned to two types of the recombination models. It is, thus, of interest to discuss

crossover of the two relaxation mechanisms. While it is ambiguous to define a critical parameter from curves of the tunneling and thermionic models in Figs. 8 and 9, it can objectively be characterized by crossing of the two lines of the exponential fits in the logarithmic plots, as shown in Fig. 7. The crossing points for each individual surface are indicated by arrows in Figs. 8 and 9. Figure 11 shows the crossing energy, V_{cross}, of the surfaces given in terms of the surface potential. Intriguingly, the V_{cross} values are concentrated at $V_s' = V_{\text{cross}} \sim 0.4$ eV in the bulk energy gap of a Si crystal ($E_g = 1.1$ eV).

In order to understand the universal V_{cross} value based on the tunneling and the thermionic models, we consider the transition during the relaxation simply by the following condition: (thermionic relaxation rate) > (tunneling relaxation
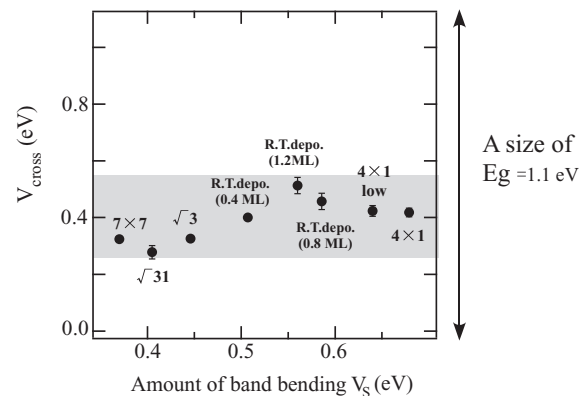

FIG. 11. V_S dependence of the surface potential that corresponds to the crossing points, V_{cross}, of the extrapolated lines of the fast and slow processes plotted in logarithmic scale, as shown in Fig. 7, for each surface.

rate). By definition of the two models,[4,6,40–44] the condition can be written in terms of τ_{tunnel} and τ_s as

$$\frac{1}{\tau_s}\exp\left(\frac{V_{SPV}(t)}{\eta kT}\right) > \frac{1}{\tau_{\text{tunnel}}}\exp\left(-\frac{2z}{a_e}\right), \tag{6}$$

which is further rewritten as

$$\frac{1}{\tau_s}\exp\left(\frac{V_s}{\eta kT}\right)\exp\left(\frac{-[V_s - V_{SPV}(t)]}{\eta kT}\right) \tag{7}$$

$$= \frac{1}{\tau_s\exp(-V_s/\eta kT)}\exp\left(\frac{-V_{\text{cross}}}{\eta kT}\right) \tag{8}$$

$$> \frac{1}{\tau_{\text{tunnel}}}\exp\left(-\frac{2z}{a_e}\right). \tag{9}$$

It is of note that, in the fundamental principle of the electron-hole recombination, decay rates of excess electrons and excess holes are equivalent. The factor, $\tau_s\exp(-V_s/\eta kT)$, remains constant due to the exponential increase of τ_s with respect to V_s, as shown in Fig. 10(c). Inserting the experimentally obtained $V_{\text{cross}} \sim 0.4$ eV and the time constant values τ_{tunnel} and τ_s, one finds the following condition at the crossing point:

$$\frac{z}{a_e} > 1\text{–}3. \tag{10}$$

This indicates that mechanisms of the relaxation switch from the tunneling to the thermionic regime when a width of the space-charge layer ($z = d$) becomes much longer than a size of the wave functions (a_e) at a surface that captures electrons from the bulk. The behavior corresponds to closing of the tunneling channel and, thus, it naturally explains the crossover to the thermionic channel. A relation between the amount of the surface potential and the size of the space-charge layer can be understood with a simulation based on the Poisson equation.[4,22] Figure 12 shows a band diagram of the space-charge layer with surface potentials of 0.4 and 0.68 eV. One can find that the layer width is longer when
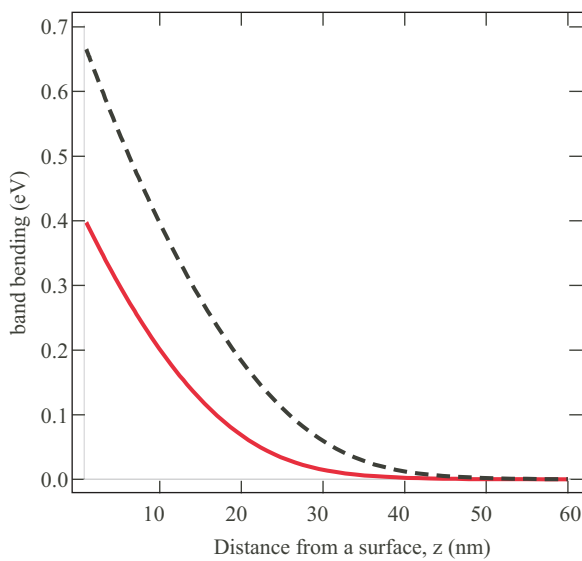

FIG. 12. (Color online) Numerical simulations of a band diagram of space-charge layers with different surface potentials, indicated by solid (red) and broken (black) curves.

the potential is larger. The amount of the surface potential (the layer width) reduces by the SPV effect and returns to the original after the relaxation. The critical value of V_{cross} corresponds to the length which breaks down the sufficient overlaps of the wave functions for the quantum tunneling transport, Eq. (10). Despite the simple analysis, the consistency in the crossover again justifies the tunneling and the thermionic recombination models for explaining relaxation of the SPV effect.

As shown in Fig. 10(d), the present analysis reveals an intriguing relation between the fast process and the surface disorder, which cannot be explained by the simple tunneling model. It is inferred that the electronic transport phenomena in the surface atomic layer play a significant role in understanding the relation. On the ordered surfaces, the surface electron transport is expected to be in the band conduction regime, while on the disordered surfaces, it is likely in the hopping regime. The difference in the surface transport mechanisms may explain the distinctive time constants between the ordered and disordered surfaces in Fig. 10(d). There is also the other uncertainty about the mechanism. The electronic states that trap electrons from the bulk spatially extend ~5 nm (a_e) toward the bulk. The trapped state is likely a surface resonance state that extends over several layers. It is also inferred that the tunneling transport may be mediated by an unoccupied state of the donor level in the space-charge layer, as shown in Fig. 1(d). Detailed information on the unoccupied surface states may be required to understand the entire mechanism.

As shown in Fig. 1, electrons transferred from the bulk recombine (non-) radiatively with the holes accumulated at the surface. The surface states at the Fermi level act as an amphoteric site for the electron-pair recombination (surface recombination). As described above, the In/Si(111) ordered phases of this study have surface states (SSs) distinct from each other. The SS of the Si(111)7 × 7 surface has dangling bond states,[38,39] while those of the 4 × 1-In phases have 1D dispersing metallic states.[36,37] Moreover, the Si(111)$\sqrt{3}$ × $\sqrt{3}$-In surface is semiconducting[38] and the surface has no metallic state. Despite the various surface-state characters of the surface phases, the time constants τ_{thermal} and τ_s show apparent dependence only on the amount of surface band bending and the surface disorder. This experimental evidence indicates the importance of these parameters in the relaxation or the carrier recombination process in the SPV in the observed time range (picoseconds to microseconds).

IV. CONCLUSION

In summary, we have carried out time-resolved photoemission experiments on various In/Si(111) surfaces with different surface parameters to investigate relaxation schemes of the surface photovoltage effect. The relaxation rate was limited by two steps of the carrier transfer from the bulk to the surface: the tunneling process at the delay time $\leqslant 100$ ns and the thermionic process on the following time scale ($\geqslant 100$). The systematic relation between the carrier dynamics and the surface parameters presented in this paper can be a guideline for designing photovoltaic or photocatalytic materials.

APPENDIX: THE TUNNELING RELAXATION MODEL

Relaxation of the surface photovoltage proceeds by recombination of photoexcited electrons and holes. The process can be quantitatively described in terms of decay of excess carriers of either holes or electrons. In the present tunneling model, the dynamical equation was formulated with the excess electrons. During the relaxation, excess holes, accumulated at the surface, recombine with excess electrons that tunnel through the surface potential barrier. To unveil the detailed mechanism, we deconvolute the model into the two processes, as shown in Fig. 1(d): (i) tunneling transport of electrons from the bulk to the surface through the space-charge layer (through the surface potential) and (ii) the electron-hole recombination at the surface. Recalling Eq. (3), the tunneling model can be formulated under the relaxation time approximation with recombination rate $(1/\tau_{\text{tunnel}})$ of process (ii), which is imposed with the exponential factor of the tunneling transport $[\exp(-\frac{2z}{a_e})]$ for process (i).

The potential variation by the carrier dynamics in the tunneling model can be obtained from the Poisson equation $\Delta\phi(z,t) = \Delta V(z,t)/e = -eN(z,t)/\epsilon\epsilon_0$. The charge density, determined from Eq. (3), is expressed as

$$N(z,t) = n(z)\exp\left\{-\frac{t}{\tau_{\text{tunnel}}}\exp\left(-\frac{2z}{a_e}\right)\right\}, \quad \text{(A1)}$$

where $n(z)$ is the initial density distribution for excess carriers. To obtain Eq. (4), we have adopted a method using the "sharp-front approximation (Fig. 13)."[42,44]

Along the surface normal (z), the double exponential function appears as integrand

$$V(t) = -\frac{e^2}{\epsilon\epsilon_0}\int_0^d dz'\int_0^{z'} n(z)\exp\left\{-\frac{t}{\tau_{\text{tunnel}}}\exp\left(-\frac{2z}{a_e}\right)\right\}dz, \quad \text{(A2)}$$
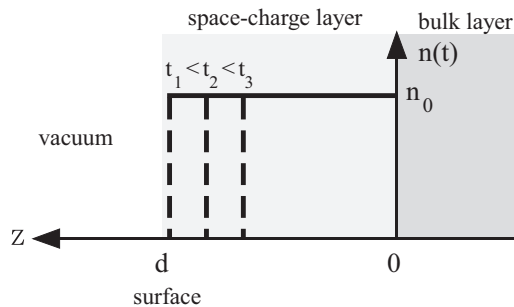

space-charge layer   bulk layer

FIG. 13. A schematic drawing of temporal variation of excess electron density distribution under the sharp-front approximation.

where z is the spatial coordinate directed from the surface and $z = 0$ is taken at the interface between the space-charge layer and the bulk layer. Under the sharp-front approximation, a front shape of the charge density toward the surface varies by the photoexcitation, followed by formation of the sharp front after the relaxation of several τ_{tunnel}'s. At times t, all the carriers after $t + \tau_{\text{tunnel}}$ are assumed to have recombined. The time constant at the front is expressed as $\tau_{\text{tunnel}}\exp\{2[d - z_0(t)]/a_e\} = t + \tau_{\text{tunnel}}$, where d corresponds to width of the space-charge layer or a layer of the surface potential barrier, and

$$z_0(t) = d - \frac{a_e}{2}\ln\left(1 + \frac{t}{\tau_{\text{tunnel}}}\right). \quad \text{(A3)}$$

This approximation is taken for time longer than the diffusion of excited electrons (roughly longer than picoseconds) and it is not valid for time just after $t = 0$. We then consider only the excess carriers within the space-charge layer.

$$n(z) = n_0, \qquad 0 < z < d \quad \text{(A4)}$$

$$= 0, \qquad z > d \quad \text{(A5)}$$

where n_0 is taken as a constant. The integral in Eq. (A2) can be given by

$$\int_0^{z'} n_0\exp\left\{-\frac{t}{\tau_{\text{tunnel}}}\exp\left(-\frac{2z}{a_e}\right)\right\} dz = n_0z', \quad 0 \leqslant z \leqslant z_0 \quad \text{(A6)}$$

$$= n_0z_0, \qquad z_0 \leqslant z \leqslant d. \quad \text{(A7)}$$

The following integration is taken for the two different spatial regions with different integrands:

$$V(t) = -\frac{e^2}{\epsilon\epsilon_0}\left(\int_0^{z_0} n_0z'dz' + \int_{z_0}^d n_0z_0dz'\right) \quad \text{(A8)}$$

$$= -\frac{e^2n_0z_0}{\epsilon\epsilon_0}\left(d - \frac{z_0}{2}\right). \quad \text{(A9)}$$

Inserting (A3), the time dependence of the potential in the tunneling model $V_{\text{tunnel}}(t)$ is expressed by definition as

$$V_{\text{tunnel}}(t) = -V(t) = \frac{e^2n_0d^2}{2\epsilon\epsilon_0}\left[1 - \left(\frac{a_e}{2d}\right)^2\ln^2\left(1 + \frac{t}{\tau_{\text{tunnel}}}\right)\right]. \quad \text{(A10)}$$

It is of note that one can obtain the same formula[44] of time dependence for the excess hole density $P(z,t)$. One simply replaces $n(z)$ and a_e with the hole density gathered at the surface, $p(z)$, and the Bohr radius of the hole state that captures an electron, a_h, respectively. The long-time approximation should logically be considered as the time longer than the transition of holes to the recombination center [Fig. 1(d)].

*imatsuda@issp.u-tokyo.ac.jp

[1] M. Grätzel, Nature (London) **414**, 338 (2001).

[2] A. Kudo and Y. Miseki, Chem. Soc. Rev. **38**, 253 (2009).

[3] H. C. Gatos and J. Lagowski, J. Vac. Sci. Technol. **10**, 130 (1973).

[4] S. M. Sze and Kwok K. Ng, *Physics of Semiconductor Devices* (Wiley, New York, 2007).

[5] S. M. Sze (ed.), *Modern Semiconductor Device Physics* (Wiley, New York, 1998).

[6] D. Bröcker, T. Gießel, and W. Widdra, Chem. Phys. **299**, 247 (2004).

[7] M. Marsi, M. E. Couprie, L. Nahon, D. Garzella, T. Hara, R. Bakker, M. Billardon, A. Delboulbe, G. Indlekofer, and A. Taleb-Ibrahimi, Appl. Phys. Lett. **70**, 895 (1997).

[8] T. E. Glover, G. D. Ackermann, Z. Hussain, and H. A. Padmore, J. Mod. Opt. **51**, 2805 (2004).

[9] W. Widdra, D. Bröcker, T. Gießel, I. V. Hertel, W. Krüger, A. Liero, F. Noack, V. Petrov, D. Pop, P. M. Schmidt, R. Weber, I. Will, and B. Winter, Surf. Sci. **543**, 89 (2003).

[10] P. D. J. Calcott, K. J. Nash, L. T. Canham, M. J. Kane, and D. Brumhead, J. Phys.: Condens. Matter **5**, L91 (1993).

[11] C. V. Shank, R. Yen, and C. Hirlimann, Phys. Rev. Lett. **50**, 454 (1983).

[12] J. E. Demuth, W. J. Thompson, N. J. DiNardo, and R. Imbihl, Phys. Rev. Lett. **56**, 1408 (1986).

[13] M. Alonso, R. Cimino, and K. Horn, Phys. Rev. Lett. **64**, 1947 (1990).

[14] R. J. Hamers and K. Markert, Phys. Rev. Lett. **64**, 1051 (1990).

[15] J. P. Long, H. R. Sadeghi, J. C. Rife, and M. N. Kabler, Phys. Rev. Lett. **64**, 1158 (1990).

[16] M. Mauerer, I. L. Shumay, W. Berthold, and U. Höfer, Phys. Rev. B **73**, 245305 (2006).

[17] N. J. Halas and J. Bokor, Phys. Rev. Lett. **62**, 1679 (1989).

[18] M. W. Rowe, H. Liu, G. P. Williams, Jr., and R. T. Williams, Phys. Rev. B **47**, 2048 (1993).

[19] M. Kamada, J. Murakami, S. Tanaka, S. D. More, M. Itoh, and Y. Fujii, Surf. Sci. **454**, 525 (2000).

[20] S. Tanaka, S. D. More, J. Murukami, M. Itoh, Y. Fujii, and M. Kamada, Phys. Rev. B **64**, 155308 (2001).

[21] A. Zangwill, *Physics at Surfaces* (Cambridge University Press, Cambridge, UK, 1988).

[22] H. Lüth, *Solid Surfaces, Interfaces and Thin Films* (Springer, New York, 2001).

[23] I. Matsuda and S. Hasegawa, J. Phys.: Condens. Matter **19**, 355007 (2007).

[24] I. Matsuda, T. Hirahara, M. Konishi, C. Liu, H. Morikawa, M. D'angelo, S. Hasegawa, T. Okuda, and T. Kinoshita, Phys. Rev. B **71**, 235315 (2005).

[25] M. Ogawa, S. Yamamoto, Y. Kousa, F. Nakamura, R. Yukawa, A. Fukushima, A. Harasawa, H. Kondo, Y. Tanaka, A. Kakizaki, and I. Matsuda, Rev. Sci. Instrum. **83**, 023109 (2012).

[26] S. Yamamoto and I. Matsuda, J. Phys. Soc. Jpn. **82**, 021003 (2013).

[27] F. Polack, M. G. Silly, C. Chauvet, B. Lagarde, N. Bergeard, M. Izquierdo, O. Chubar, D. Krizmancic, M. Ribbens, J.-P. Duval, C. Basset, S. Kubsky, F. Sirotti, R. Garrett, I. Gentle, K. Nugent, and S. Wilkins, *The 10th International Conference on Synchrotron Radiation Instrumentation*, AIP Conf. Proc. 1234 (AIP, Melville, NY, 2010), p. 185.

[28] N. Bergeard, M. G. Silly, D. Krizmancic, C. Chauvet, M. Guzzo, J. P. Ricaud, M. Izquierdo, L. Stebel, P. Pittana, R. Sergo, G. Cautero, G. Dufour, F. Rochet, and F. Sirotti, J. Synchrotron Radiat. **18**, 245 (2011).

[29] S. Takeda, X. Tong, S. Ino, and S. Hasegawa, Surf. Sci. **415**, 264 (1998).

[30] H. M. Zhang, K. Sakamoto, G. V. Hansson, and R. I. G. Uhrberg, Phys. Rev. B **78**, 035318 (2008).

[31] F. J. Himpsel, G. Hollinger, and R. A. Pollak, Phys. Rev. B **28**, 7014 (1983).

[32] J. J. Lander and J. Morrison, J. Appl. Phys. **36**, 1706 (1965).

[33] J. Kraft, M. G. Ramsey, and F. P. Netzer, Phys. Rev. B **55**, 5384 (1997).

[34] A. V. Zotov, A. A. Saranin, O. Kubo, T. Harada, M. Katayama, and K. Oura, Appl. Surf. Sci. **159–160**, 237 (2000).

[35] A. A. Saramin, A. V. Aotov, A. N. Tovpik, M. A. Cherevik, E, N. Chukurov, V. G. Lifshits, M. Katayama, and K. Oura, Surf. Sci. **450**, 34 (2000).

[36] H. W. Yeom, S. Takeda, E. Rotenberg, I. Matsuda, K. Horikoshi, J. Schaefer, C. M. Lee, S. D. Kevan, T. Ohta, T. Nagao, and S. Hasegawa, Phys. Rev. Lett. **82**, 4898 (1999).

[37] T. Abukawa. F. Hisamatsu, T. Goto, S. Kono, M. Sasaki, T. Kinoshita, and A. Kakizaki, Surf. Sci. **325**, 33 (1995).

[38] R. I. G. Uhrberg and G. V. Hansson, Crit. Rev. Solid State Mater. Sci. **17**, 133 (1991).

[39] R. Losio, K. N. Altmann, and F. J. Himpsel, Phys. Rev. B **61**, 10845 (2000).

[40] E. F. Schubert, A. Fischer, and K. Ploog, Phys. Rev. B **31**, 7937 (1985).

[41] S. Tokudomi, J. Azuma, K. Takahashi, and M. Kameda, J. Phys. Soc. Jpn. **77**, 14711 (2008).

[42] H. J. Queisser and D. E. Theodorou, Phys. Rev. B **33**, 4027 (1986).

[43] M. Ogawa, S. Yamamoto, R. Yukawa, R. Hobara, C.-H. Lin, R.-Y. Liu, S.-J. Tang, and I. Matsuda, Phys. Rev. B **87**, 235308 (2013).

[44] Th. Dittrich, V. Duzhko, F. Koch, V. Kytin, and J. Rappich, Phys. Rev. B **65**, 155319 (2002).

[45] L. Kronik and Y. Shapira, Surf. Sci. Rep. **37**, 1 (1999).